Chaos for cardiac arrhythmias through a one-dimensional modulation equation for alternans

Shu Dai[1] and David G. Schaeffer[2]
[1]*Mathematical Biosciences Institute, The Ohio State University, Columbus, Ohio 43210, USA*
[2]*Department of Mathematics and Center for Nonlinear and Complex Systems, Duke University, Durham, North Carolina 27708, USA*

(Received 23 December 2009; accepted 1 June 2010; published online 30 June 2010)

Instabilities in cardiac dynamics have been widely investigated in recent years. One facet of this work has studied chaotic behavior, especially possible correlations with fatal arrhythmias. Previously chaotic behavior was observed in various models, specifically in the breakup of spiral and scroll waves. In this paper we study cardiac dynamics and find spatiotemporal chaotic behavior through the Echebarria–Karma modulation equation for alternans in one dimension. Although extreme parameter values are required to produce chaos in this model, it seems significant mathematically that chaos may occur by a different mechanism from previous observations. © *2010 American Institute of Physics*. [doi:10.1063/1.3456058]

Cardiac arrhythmias—interruption of the normal electrical rhythms of the heart—can be life-threatening, especially if they lead to ventricular fibrillation. It is believed that ventricular fibrillation is characterized by chaotic dynamics of the heart. Spatially discordant alternans, a period-doubling response of the heart to rapid pacing, has been regarded as a precursor of chaotic behavior. A modulation-equation approximation for the spatiotemporal development of alternans in a cardiac fiber was constructed by Echebarria and Karma. Both steady-state and Hopf bifurcations have been observed in this equation. In the present paper, we show that there also exist chaotic solutions of this equation in one-dimensional fiber, which is a different origin of chaos from previous observations.

I. INTRODUCTION

It is believed that ventricular fibrillation in cardiac tissue represents chaotic behavior of the system.[1] In two and three dimensions chaos has been seen in the breakup of spiral and scroll waves in an excitable medium.[2,3] In low dimensions (0 and 1) cardiac chaos was also widely investigated.[4–7] Recent studies show that alternans, a bifurcation of the action potential duration (APD) in cardiac cells in which short and long APDs alternate under rapid pacing, may be a precursor of ventricular fibrillation.[8–13] The transition to cardiac chaos may be various, typical causes of which were summarized in Ref. 5: memory effect,[14] nonmonotonic restitution,[6] conduction block,[4,5] and spatial variability in high dimensions.[7] In this paper, through the Echebarria–Karma modulation equation, we show a quasiperiodic transition to chaos of the alternans in one-dimensional fiber, in spirit of Ruelle–Takens–Newhouse route.[15–17] We note that we assume the restitution curve is monotone without memory and no block appears in the dynamics. Although parameter values in the modulation equation for the chaotic solution to exist may be too extreme for ionic models, we mathematically provide a possible different mechanism for cardiac chaos.

In a single cell, the dynamics of APDs undergoes a period-doubling bifurcation to alternans under rapid pacing. In extended tissue, where we assume there is no conduction block (every stimulus yields a successfully propagating action potential), the amplitude and phase of alternans typically depend on both position and time. In the case of a one-dimensional cardiac fiber with stimuli applied at one end, under a weakly nonlinear approximation, Echebarria and Karma[18] derived a modulation equation to describe the evolution of alternans along the fiber in simple mapping models (see Sec. II for a short review of this equation). For certain values of the parameters in the equation, the solution is chaotic.

The organization of this paper is as follows. In Sec. II, we review the modulation equation derived in Ref. 18, including its early bifurcations.[19] In Sec. III, choosing one set of (extreme) parameter values as an example, we show that solutions of the modulation equation are chaotic. Our results are discussed in Sec. IV.

II. THE MODULATION EQUATION AND ITS EARLY BIFURCATIONS

The Echebarria–Karma[18] theory extends the pioneering model[20,23] for restitution in a single cardiac cell,

$$A_{n+1} = f(D_n), \tag{2.1}$$

where A_n denotes the nth APD and D_n denotes the nth diastolic interval (DI), and the restitution curve f is assumed to be monotone increasing. Under repeated stimulation with period B, usually called basic cycle length (BCL), we have the relation $D_n = B - A_n$. Alternans emerge as a period-doubling bifurcation in the iteration as B decreases, say for $B < B_{\text{crit}}$.

In extended tissue action potentials propagate, and the APDs will be a function of position as well as time. In the case of one dimension, suppose a cardiac fiber of length ℓ is

stimulated periodically at one end $x=0$ with BCL B, and assume each stimulus successfully generates an action potential that propagates down the fiber. Let $A_n(x)$ be the duration of the nth action potential at the position x. If the pacing is sufficiently rapid, say $B<B_{\text{crit}}$, alternans are expected. In Ref. 21 Echebarria and Karma sought a multiscale expansion in the form

$$A_n(x) = A_{\text{crit}} - \delta A + (-1)^n a_n(x), \tag{2.2}$$

where A_{crit} is the APD when pacing with period $B=B_{\text{crit}}$, δA is the average shortening of APD resulting from decreasing B below B_{crit}, and $a_n(x)$ is the amplitude of alternans at the nth beat. It is assumed that $a_n(x)$ varies slowly from beat to beat, so that one may regard it as the discrete values of a smooth function $a(x,t)$ of continuous time t, i.e., $a_n(x)=a(x,t_n)$ where $t_n=n\cdot B$ for $n=0,1,2,\ldots$.

Based on the above assumptions, a weakly nonlinear modulation equation for $a(x,t)$ was derived in Ref. 18 which, after nondimensionalization with respect to time, is given by

$$\partial_t a = \sigma a + \xi^2 \partial_{xx} a - w \partial_x a - \Lambda^{-1} \int_0^x a(x',t)dx' - g a^3. \tag{2.3}$$

Here σ, the bifurcation parameter may be obtained by[18]

$$\sigma = \tfrac{1}{2}(B - B_{\text{crit}}) \cdot f''(D_{\text{crit}}), \tag{2.4}$$

where $D_{\text{crit}}=B_{\text{crit}}-A_{\text{crit}}$; Λ, w, ξ are positive parameters, each having the units of length that are derived from the equations of the cardiac model; and the nonlinear term $-ga^3$ limits growth after the onset of linear instability. Neumann boundary conditions

$$\partial_x a(0,t) = 0, \quad \partial_x a(\ell,t) = 0 \tag{2.5}$$

are imposed in Eq. (2.3).

To complete the nondimensionalization of Eq. (2.3), we define the following dimensionless variables:

$$\bar{\Lambda} = \Lambda \cdot w^3 \xi^{-4}, \quad \bar{x} = x \cdot w \xi^{-2}, \quad \bar{\ell} = \ell \cdot w \xi^{-2}, \tag{2.6}$$

and we rescale the time t and parameters σ and g,

$$\bar{t} = t \cdot w^2 \xi^{-2}, \quad \bar{\sigma} = \sigma \cdot w^{-2} \xi^2, \quad \bar{g} = g \cdot w^{-2} \xi^2. \tag{2.7}$$

In this notation, Eq. (2.3) may be rewritten

$$\partial_{\bar{t}} a = \bar{\sigma} a + \mathbf{L} a - \bar{g} a^3, \tag{2.8}$$

where $\mathbf{L}$ is the linear operator on the interval $0<\bar{x}<\bar{\ell}$ (with Neumann boundary conditions),

$$\mathbf{L} a = \frac{\partial^2 a}{\partial \bar{x}^2} - \frac{\partial a}{\partial \bar{x}} - \bar{\Lambda}^{-1} \int_0^{\bar{x}} a(\bar{x}')d\bar{x}'. \tag{2.9}$$

We could remove the factor $\bar{g}$ by rescaling on the amplitude $a(x,t)$, but little would be gained by this. In this paper, $\bar{g}$ is fixed at 40. For convenience below we will omit all the bars in Eqs. (2.8) and (2.9).

The trivial solution of Eq. (2.3), $a(x,t)\equiv 0$, is linearly stable for σ small (including all negative values) and loses its stability as σ increases beyond some threshold σ_{th}. Instability may appear through either a steady-state or Hopf bifurcation. Which bifurcation occurs first depends on whether $\Omega_{\max}$, the eigenvalue of $\mathbf{L}$ in Eq. (2.9) which has the largest real part, is real or complex, and

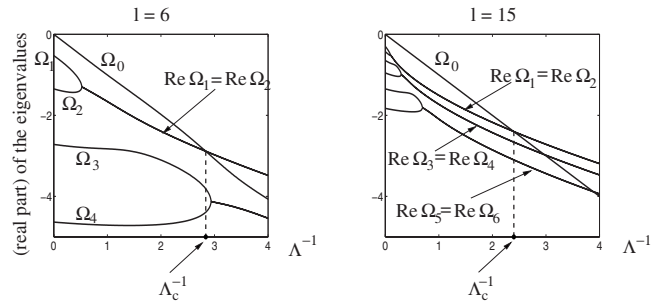

FIG. 1. The evolution of the real parts of the first few eigenvalues $\Omega_0,\Omega_1,\Omega_2,\ldots$ of the linear operator in Eq. (2.9) vs Λ^{-1} for $\ell=6$ and 15, respectively. In each case, all eigenvalues are real for Λ^{-1} sufficiently small, but, except for Ω_0, they become complex as Λ^{-1} increases. Λ_c^{-1}, which depends on ℓ, is the crossover point such that if $\Lambda^{-1}>\Lambda_c^{-1}$ the eigenvalue which has largest real part, $\Omega_{\max}$, is complex.

$$\sigma_{\text{th}} = -\operatorname{Re}\Omega_{\max}. \tag{2.10}$$

Figure 1 shows how the first few eigenvalues of $\mathbf{L}$ (only real parts are graphed) depend on the dispersive coefficient Λ^{-1}. [The figure is based on lengths $\ell=6$ and 15, but the behavior is qualitatively similar for all sufficiently large ℓ. Note that all eigenvalues lie in the (stable) left half plane.] It may be seen from the figure that there is a critical value Λ_c^{-1}, such that if $\Lambda^{-1}<\Lambda_c^{-1}$, the real eigenvalue Ω_0 of $\mathbf{L}$ has largest real part (thus steady-state bifurcation occurs first) and if $\Lambda^{-1}>\Lambda_c^{-1}$, then the complex pair $\Omega_{1,2}$ has the largest real part (thus Hopf bifurcation occurs first).

Further bifurcations occur if σ is increased beyond the first bifurcation point. In particular, for some values of Λ^{-1}, chaotic solutions emerge for sufficiently large σ. Figure 2 illustrates simulation results for the modulation equation (2.3) for $0<\Lambda^{-1}<15$ and $0<\sigma<25$, where ℓ is fixed at 15. Each marker represents that chaotic solutions are observed for the corresponding values of Λ^{-1} and σ. In Sec. III, we

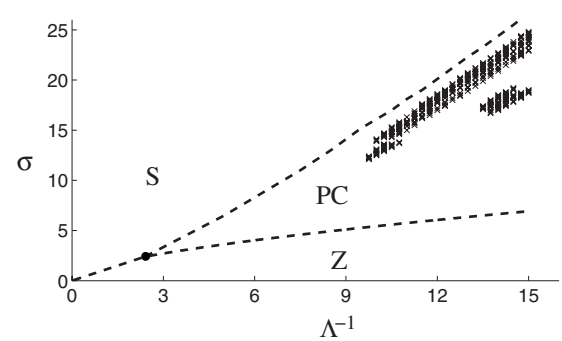

FIG. 2. Regions in parameter space (Λ^{-1},σ) where the solution of Eq. (2.3) exhibits different long-term behavior: (Z) trivial zero steady-state solutions; (S) standing wave solutions; (PC) periodic, quasiperiodic, and chaotic solutions, where markers indicate that chaotic solutions are observed. The three regions intersect at the critical value Λ_c^{-1}. The dynamics around the intersection point was investigated in our earlier paper (Ref. 22). We also note that for all Λ^{-1} we have standing wave solution eventually as σ increases.

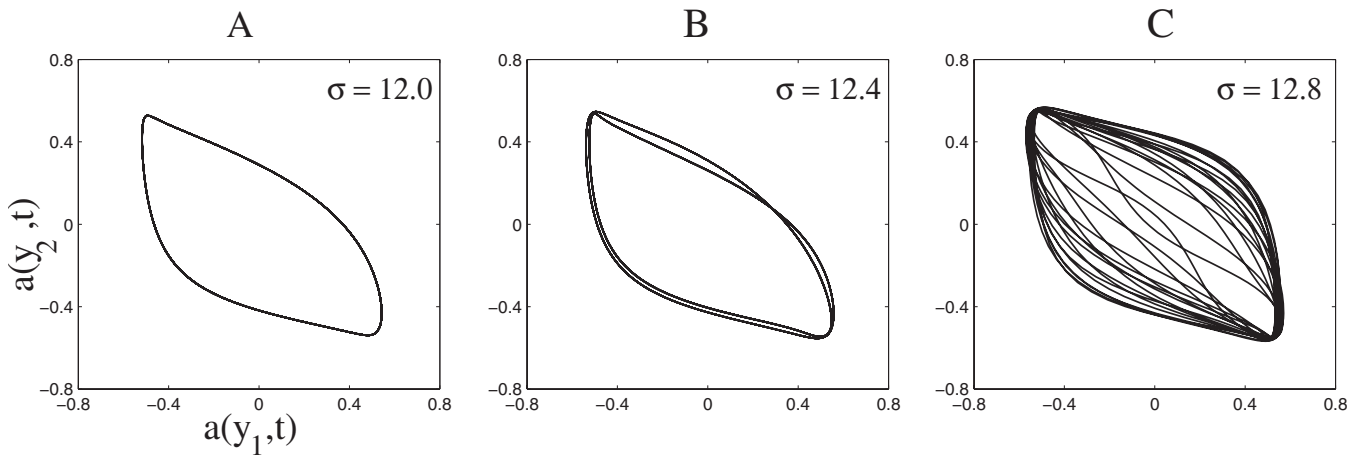

FIG. 3. Phase plane of $a(y_2,t)$ vs $a(y_1,t)$ for three different values of σ, assuming $\ell=15$ and $\Lambda^{-1}=10$.

study thoroughly one specific case $\ell=15$, $\Lambda^{-1}=10$, and $\sigma=12.8$, and we show that the nontrivial solutions to the modulation equation (2.3) are chaotic.

III. EVIDENCE OF CHAOS

Throughout this section, we assume the cardiac fiber length $\ell=15$ and the dispersive coefficient $\Lambda^{-1}=10$ (both in dimensionless units). We investigate the behavior of the solution to Eq. (2.3) for various values of σ by numerically solving the equation. The numerical method we employ is based on second order operator splitting. We separate the right-hand side of Eq. (2.8) as linear part $\sigma a+\mathbf{L}a$ and nonlinear part $-ga^3$. After spatial discretization (described below) the linear part is equivalent to a constant-coefficient linear system of ordinary differential equations, which can be solved to arbitrary order in time; and the nonlinear part can be solved analytically. We discretize the fiber by a finite difference method, i.e., if for example we have a spatial step $dx=0.075$, we have mesh points $x_{i-1/2}=(i-0.5)dx$ for $i=0,1,\ldots,200,201$. To approximate the operator $\mathbf{L}$, we use classical difference quotients for the derivatives and trapezoidal rule for the integral part to obtain second order accuracy in space. The Neumann boundary conditions (2.5) imply

$$a(x_{-1/2},t)=a(x_{1/2},t) \quad \text{and} \quad a(x_{200-1/2},t)=a(x_{201-1/2},t) \tag{3.1}$$

for all time t. For the simulations in Figs. 2–10 we use time step $dt=0.002$. And in the simulations in Figs. 7 and 8 we choose various values of dt for exploration.

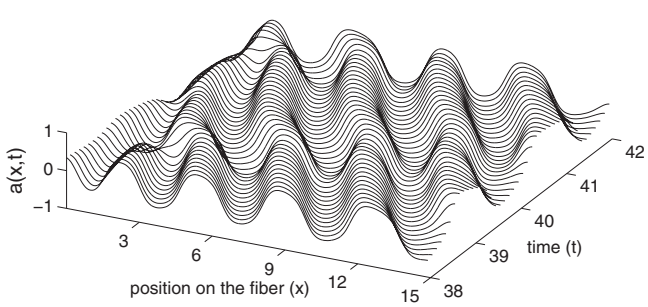

FIG. 4. Space-time plot of $a(x,t)$ obtained by simulations of Eq. (2.3) for $\ell=15$, $\Lambda^{-1}=10$, and $\sigma=12.8$.

In Fig. 3 we show a phase-plane representation of the solutions to Eq. (2.3) for several different values of σ, choosing two fixed positions y_1 and y_2 on the fiber and then plotting $a(y_2,t)$, $a(y_1,t)$ as time evolves. For instance in Fig. 3, we use $y_1=x_{150-1/2}$ and $y_2=x_{170-1/2}$. It appears A is a periodic solution, B is period doubled, and C is possibly chaotic. Figure 4 shows a space-time plot of $a(x,t)$ for the possible chaotic solution when $\sigma=12.8$.

To view the evolution of the dynamics as σ increases more clearly, we draw the orbit diagram in Fig. 5, which is obtained by the following steps. For each value of σ, consider the Poincaré sectional hyperplane defined by $a(y_2,\cdot)=0$. We study the solution of Eq. (2.3) in a time range $T_1<t<T_2$, where $T_1=200$ is chosen to eliminate the initial transient and $T_2=700$. For times in this interval, if the solution $a(x,t)$ transverses this hyperplane at some time t_n in the positive direction, i.e., $a(y_2,\cdot)$ increasing from negative to positive at time t_n, we record the value of $a(y_1,t_n)$ in Fig. 5. Therefore, if the solution is "period-one" as in Fig. 3(a), we obtain one value of $a(y_1,\cdot)$; if the solution is "period-two" as in Fig. 3(b), we obtain two distinct values of $a(y_1,\cdot)$; and if the solution is chaotic as in Fig. 3(c), we expect to obtain a large number of values, depending on the range of time we consider. The orbit diagram in Fig. 5 is given by plotting all the values of $a(y_1,t_n)$ we obtain versus σ.

From the orbit diagram, we find that as σ increases, there is a period-two bifurcation at around $\sigma=12.20$, and a bifurcation to intermittent chaos at around $\sigma\approx 12.44$. The intermittency can be observed by plotting the values $a(y_1,t_n)$ versus n in Fig. 6, where $\sigma=12.45$ is just beyond the bifurcation value.

We observe that there is a chaotic window $12.45\lesssim\sigma\lesssim 13.12$ in the orbit diagram. We have examined the range for σ between 13.03 and 13.06, the "gap" in the chaotic window shown in the diagram, in detail. In particular, (i) increasing σ in steps of 10^{-6}, we found various periodic solutions. The period farthest along in the U-sequence[24,25] was nine; (ii) in certain ranges a period four solution was ob-

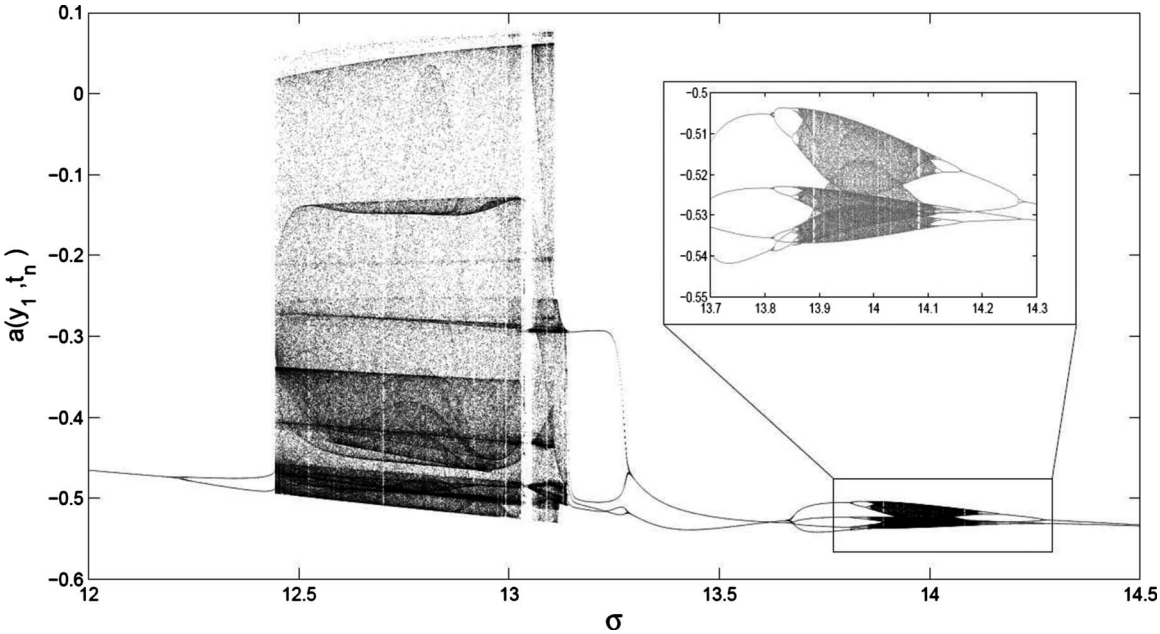

FIG. 5. Orbit diagram for the solution to Eq. (2.3) as σ increases, assuming $\ell=15$ and $\Lambda^{-1}=10$. The interval between two adjacent σ's is 0.001. As explained in the text, the vertical axis is $a(y_1,t_n)$, where t_n is some time between $T_1=200$ and $T_2=700$ when $a(y_2,t)$ becomes positive.

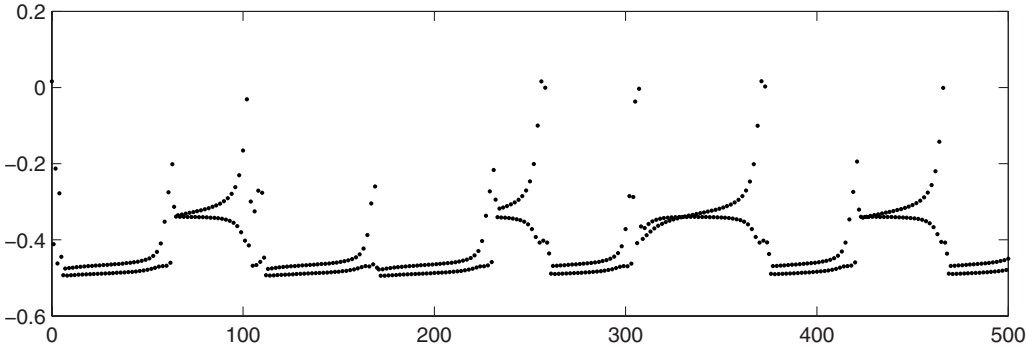

FIG. 6. Plotting of the values $a(y_1,t_n)$ in the Poincaré hyperplane vs n, where $\sigma=12.45$, which is just beyond the bifurcation point. An intermittent pattern is apparent.

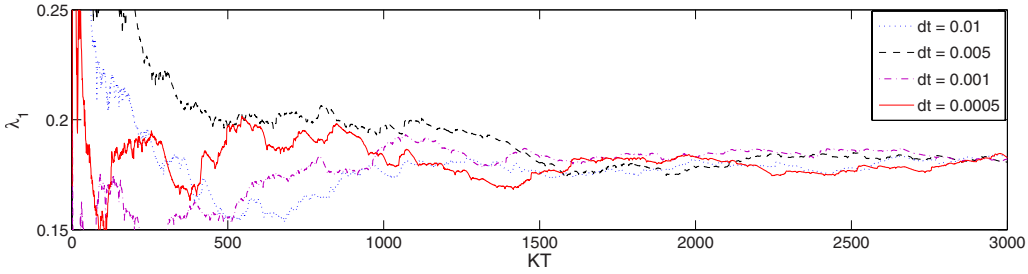

FIG. 7. (Color online) The first Lyapunov exponent λ_1 vs the total time KT for the computation, where $\ell=15$, $\Lambda^{-1}=10$, and $\sigma=12.8$.

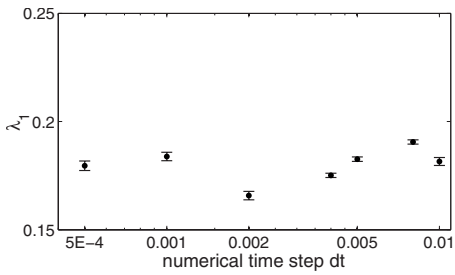

FIG. 8. The averaged first Lyapunov exponent λ_1 during $2500 \leq KT \leq 3000$ vs numerical time step dt, where $\ell=15$, $\Lambda^{-1}=10$, and $\sigma=12.8$.

served at all points, but the precise orbit seemed to jump in a discontinuous fashion.

For σ beyond 13.12, the solution exhibits more transitions between chaotic and periodic behaviors. The orbit diagram in Fig. 5 provides an elementary overview of the behavior of the solution. However, to verify that we do have a chaotic solution indeed, we need more evidence. We study the case $\sigma=12.8$ in detail in the following.

A. Computing the Lyapunov exponents

The most straightforward approach to verify chaos is to show that the first Lyapunov exponent of the system is positive.[26] The first Lyapunov exponent can be simply obtained by considering the variation equation of Eq. (2.3), i.e.,

$$\partial_t \delta a = \sigma \delta a + \mathbf{L}\delta a - 3ga^2(x,t)\delta a, \tag{3.2}$$

where $a(x,t)$ is the solution to Eq. (2.3). To perform the computation, we choose an initial state $a_0=a(x,t_0)$ lying in

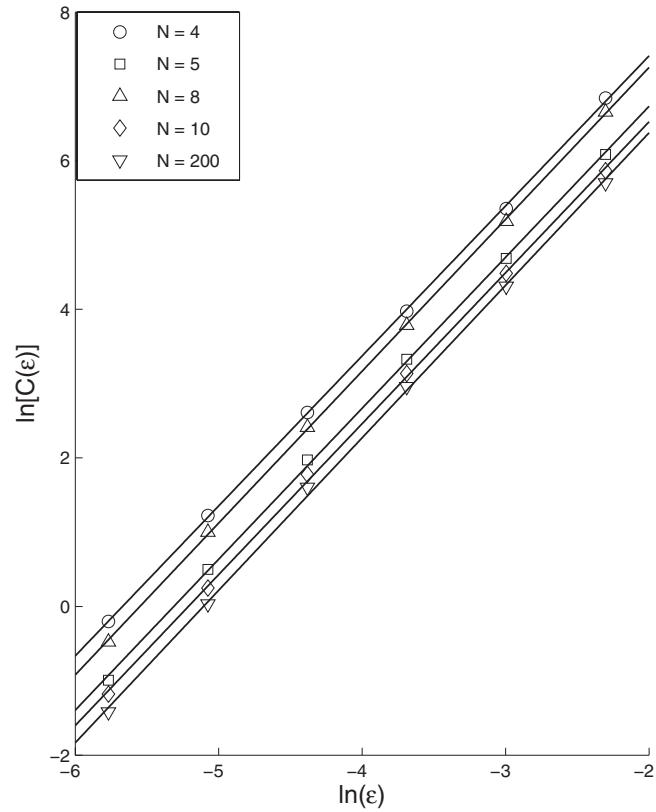

FIG. 10. Plot of the logarithm of $C(\epsilon)$, the average of number of points on the trajectory falling into the ϵ-balls, vs logarithm of ϵ, for various N, the number of spatial subintervals in approximating the $L^2(0,\ell)$-norm in Eq. (3.3). Note that in the cases of $N=20,50,100$, the plots are very close to the case $N=200$ and hard to distinguish. Therefore, they are not plotted individually.

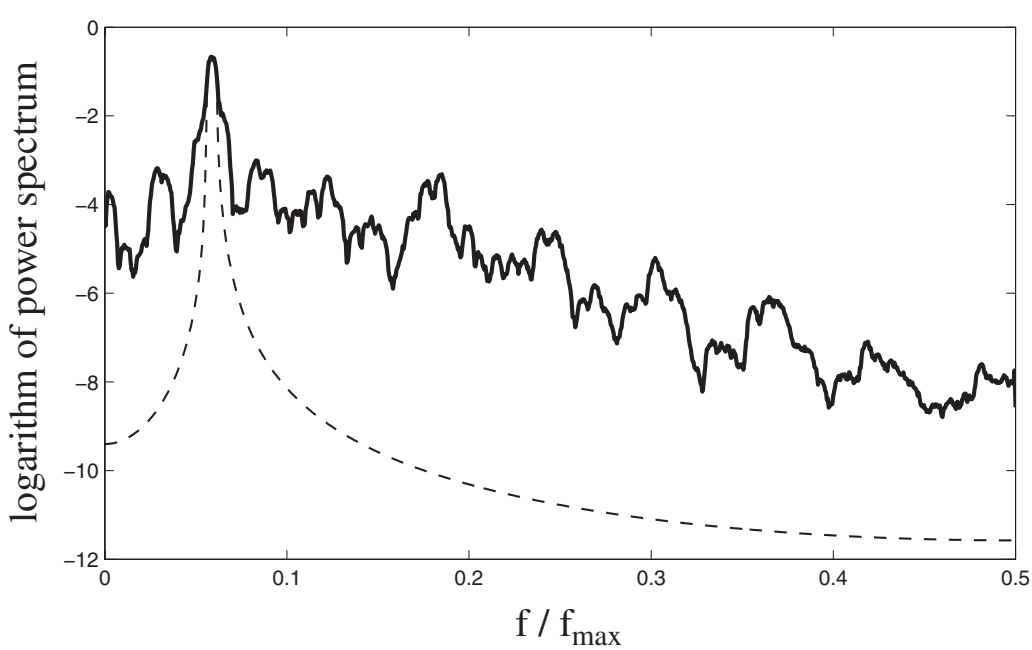

FIG. 9. Plot of the logarithm of the power spectrum vs the frequency. The solid curve is for the solution $a(y_1,t_k)$ with fixed position $y_1=x_{150-1/2}$ and total 2048 discrete t_k's by time interval 0.1, assuming $\ell=15$, $\Lambda^{-1}=10$, and $\sigma=12.8$; the dashed curve is the instrumentally sharp spectrum.

the basin of the attractor and an initial variation $u^{(0)} := \delta a_0$ (usually normalized). For a fixed time length T, we integrate the variation Eq. (3.2) to obtain δa_1. We then normalize δa_1 to obtain $u^{(1)} = \delta a_1 / \|\delta a_1\|$, where the norm of a function on the fiber $f(x)$ is defined to be the L^2-norm, i.e.,

$$\|f\| := \left(\int_0^\ell |f(x)|^2 dx \right)^{1/2}. \tag{3.3}$$

We then integrate the variation equation with initial condition $u^{(1)}$ to obtain δa_2. We repeat the procedure K times, and for K large enough, we obtain the estimate[27]

$$\lambda_1 \approx \frac{1}{KT} \sum_{j=1}^{K} \ln \|\delta a_j\|. \tag{3.4}$$

Figure 7 shows the right-hand side of Eq. (3.4) versus the total time KT for $T=1$ with different numerical time steps dt. Using Eq. (3.4), we estimate that the first Lyapunov exponent λ_1 is roughly in the range (0.16, 0.2), which is positive. Significantly, λ_1 does not show any tendency to decrease to zero as KT tends to infinity. Incidentally, the second Lyapunov exponent λ_2 is approximately zero (error within 10^{-3}).

For further evidence, we refer to Fig. 8, which is a plot of λ_1 versus various numerical time steps dt. We observe that there is apparently no trend for λ_1 to vanish for smaller time step.

Also, the computation of λ_1 does not depend on the length of the normalization time interval T, provided T is not too large. To check this we repeated the previous calculation for $T=1,2,4,8,16$ with fixed total time KT and observed very little difference.

B. Power spectrum

As supplementary evidence we show that the trajectory has a continuous power spectrum. Specifically, from a sequence $\{t_k\}$ of equally spaced times $\Delta t = 0.1$ (starting after the transient has decayed), we obtain the time sequence $\{a(y_1, t_k)\}$, and we perform a discrete Fourier transformation to the time sequence $\{a(y_1, t_k)\}$. In practice, we collect 2048 values of $a(y_1, t_k)$ in total and multiply the time sequence $\{a(y_1, t_k)\}$ by a masking function $k/2048(1-k/2048)$ to make the periodic extension of the sequence continuous. Figure 9 shows a plot of the logarithm of the amplitude versus the frequency (solid curve), where each value has been averaged over its ten nearest neighbors. We observe that the spectrum has a continuous pattern.

For comparison, we plot the instrumentally sharp spectrum on the same graph (dashed curve, only first harmonic is plotted), which is generated as follows. We consider the pure periodic time sequence $\{A \cos(\omega t_k)\}$, where ω is the frequency of the power spectrum of $\{a(y_1, t_k)\}$ with largest amplitude (cf. Fig. 9), and A is the corresponding amplitude. We then obtain the power spectrum of $\{A \cos(\omega t_k)\}$ with the same masking process.

TABLE I. The correlation dimension of the attractor of the solution to Eq. (2.3) for various N, the number of spatial subintervals in approximating $L^2(0,\ell)$-norm in Eq. (3.3), assuming $\ell=15$, $\Lambda^{-1}=10$, and $\sigma=12.8$.

N	Dimension
4	2.018 ± 0.012
5	2.031 ± 0.020
8	2.043 ± 0.012
10	2.031 ± 0.021
20	2.049 ± 0.026
50	2.052 ± 0.027
100	2.052 ± 0.027
200	2.052 ± 0.027

C. The correlation dimension of the attractor

Further information is provided by the correlation dimension[28] of the attractor of the trajectory. We calculate the correlation dimension following Refs. 26 and 29. Let p be a "base point" obtained by letting the system evolve for a long time such that the transient decays. Consider a ball $B_p(\epsilon)$ centered at p with radius ϵ, where the distance between two solutions at time t, say $a(x,t)$ and $b(x,t)$, is given by the $L^2(0,\ell)$-norm. Then we generate a large number (5×10^5) of points on the trajectory, a time sequence with equal time interval ΔT. Let $n(\epsilon)$ be the number of these points located in the ball $B_p(\epsilon)$. If the attractor is D-dimensional, we expect $n(\epsilon)$ to be approximately proportional to ϵ^D, i.e., there is some constant C such that

$$n(\epsilon) \approx C\epsilon^D. \tag{3.5}$$

In case that the solution is periodic, the dimension of the attractor D is exactly 1. In general, to find the dimension, we rewrite Eq. (3.5) in the following form:

$$\ln(n(\epsilon)) \approx D \ln(\epsilon) + \ln C, \tag{3.6}$$

i.e., $\ln(n(\epsilon))$ is expected to be a linear function of $\ln(\epsilon)$ with slope D that may be estimated from data.

For better accuracy, we pick 1000 base points on the attractor and take $n(\epsilon)$ as the average of the slopes obtained by the above procedure. In Fig. 10, for $\epsilon_k = 2^{-k}\epsilon_0$ where $k=0,1,2,\ldots$, we plot $\ln(n(\epsilon_k))$ versus $\ln(\epsilon_k)$. For the case labeled $N=200$ we find that the correlation dimension $D \approx 2.052 \pm 0.027$. The standard deviation in D arises from the simple linear regression method, which assumes the errors are independent Gaussians.

We now explain the meaning of N in Fig. 10 and Table I. In the above calculation, the distance between two "points," which are in fact two functions $a(\cdot,t_1)$ and $a(\cdot,t_2)$, is defined by the $L^2(0,\ell)$-norm. In the numerical simulation, we only have the function values on the spatial mesh points, i.e., $a(x_{j-1/2},t)$ for $j=0,1,\ldots,200,201$. With trapezoidal rule, we find the $L^2(0,\ell)$-norm defined in Eq. (3.3) is approximated by

TABLE II. The correlation dimension of the attractor of the solution to Eq. (2.3) for various ℓ, assuming $\Lambda^{-1}=10$ and $\sigma=12.8$.

Length ℓ	Dim D
6	2.020 ± 0.025
9	1.992 ± 0.031
12	1.939 ± 0.012
15	2.052 ± 0.027
18	1.935 ± 0.010
21	2.099 ± 0.030

$$\|a(\cdot,t)\| = \left(\int_0^{\ell} |a(x,t)|^2 dx\right)^{1/2} \approx \sqrt{dx}\left(\sum_{i=1}^{200} a(x_{i-1/2},t)^2\right)^{1/2}, \tag{3.7}$$

where we have used the boundary conditions (3.1). Therefore, up to a constant factor, the $L^2(0,\ell)$-norm is equal to the Euclidean distance of points in a 200-dimensional Euclidean space. For comparison, we also consider calculating the norm using only a subgrid. To avoid unnatural interpolation, we consider subgrids with values of N that divide 200. The data are plotted in Fig. 10 and the dimension D is summarized in Table I. We find that in all cases, D is nearly 2.

IV. DISCUSSION

We have studied numerically chaotic solutions in one case of the Echebarria–Karma modulation equation (2.3) for APD alternans propagating on a cardiac fiber, specifically with dimensionless parameters $\ell=15$, $\Lambda^{-1}=10$, and $\sigma=12.8$. We verified that this solution is indeed chaotic by showing that (i) the first Lyapunov exponent of the solution is positive and (ii) the power spectrum is continuous.

Above we described computations showing that the correlation dimension of the attractor for these parameter values is slightly larger than 2. We have also investigated how the correlation dimension depends on the length ℓ; the results, including the previous case $\ell=15$, are presented in Table II. In all cases we keep $\Lambda^{-1}=10$ and $\sigma=12.8$, the solutions are all chaotic, and we use the $L^2(0,\ell)$-norm in computing the distance between trajectories. As we mentioned before, in estimating the dimensions by linear regression, the errors are assumed to be independent Gaussians. Of course this assumption need not hold; indeed, there may even be nonrandom systematic errors, especially for intermittent chaos. Thus the actual errors could significantly exceed these estimates. Despite these qualifications, it does seem that the dimension does not increase with ℓ, in contrast, for example, to the problem considered in Ref. 30.

If the error estimates in Table II are reliable, then two of the dimensions are less than 2, which would contradict the Kaplan–Yorke conjecture.[31,32] According to this conjecture, the correlation dimension of an attractor equals the Lyapunov dimension,[31] the latter being defined as

$$D_L = k + \frac{\lambda_1+\lambda_2+\cdots+\lambda_k}{|\lambda_{k+1}|}, \tag{4.1}$$

where λ_j's are the Lyapunov exponents and k the maximum value of j such that $\lambda_1+\lambda_2+\cdots+\lambda_j>0$. Of course $\lambda_1>0$ and $\lambda_2\geq 0$, so $k\geq 2$ and hence $D_L>2$. Although the Kaplan–Yorke conjecture has been proved in certain special cases,[33,34] it has not been proved in general. Thus, in the present problem it would not contradict any known results to encounter a correlation dimension less than 2.

The values of the parameters to observe chaos are extreme. In particular, the value of σ is far beyond the first bifurcation and may be unphysical. We now relate our previous results to ionic models. We consider two typical ionic models: Noble's model[35] and two-current model.[36] In the following discussion, the parameters without bars are dimensional before the scaling (2.6) and (2.7). Values of the parameters for each model are given in Table III. For Noble's model, since $\bar{\Lambda}^{-1}<\bar{\Lambda}_c^{-1}$, under rapid pacing the alternans along the fiber have a pattern of standing wave always (assuming no conduction block), which matches the simulation results. An illustration of the simulation may be found in Ref. 18. For two-current model, which has $\bar{\ell}=8.86$ and $\bar{\Lambda}^{-1}=48.4$., chaotic solutions of the modulation equation (2.3) exist for some values of $\bar{\sigma}$ greater than $\bar{\sigma}_{\text{chaos}}\approx 104.6$, which requires the BCL to be reduced to a threshold by Eq. (2.4). Simulations of two-current model (see Appendix of Ref. 19 for detail of the model) show that $f''(D_{\text{crit}})\approx -0.020$ ms^{-1} and $B_{\text{crit}}\approx 370$ ms. Therefore, by Eqs. (2.4) and (2.7), to obtain chaos we need to reduce B to 244 ms. However, this BCL is too small and it causes block (2:1 response), which contradicts the assumption of the modulation equation (we note that the minimal value of BCL for no block is about 320 ms). This explains why we do not observe chaos in the simulation when we decreases B until conduction block occurs. An example of the simulation which shows a periodic pattern is given in Ref. 19. Although it seems in the above two models the parameter values for chaotic solutions are unphysical, we provide mathematically a different mechanism for the cardiac chaos.

It is also worthwhile to discuss the effect of coupling strength between cells. Stronger coupling corresponds to larger conductance of gap junctions[37] between cells, which

TABLE III. Values of parameters for Noble's model and two-current model from Ref. 18 and Table I in Ref. 19: w, ξ, Λ^{-1}, and ℓ have units of length in centimeter; $\bar{\ell}$ and $\bar{\Lambda}^{-1}$ are dimensionless variables defined in Eq. (2.6); $\bar{\Lambda}_c^{-1}$ is the dimensionless critical value, as shown in Fig. 1.

Model	w	ξ	Λ^{-1}	$\bar{\Lambda}^{-1}$	ℓ	$\bar{\ell}$	$\bar{\Lambda}_c^{-1}$
Noble	0.045	0.180	0.020	0.23	20	27.78	2.27
Two-current	0.034	0.310	0.206	48.4	25	8.84	2.67

results in a larger effective diffusion coefficient K in the spirit of homogenization.[38] The parameters w, ξ, and Λ^{-1} may be obtained by[18,21]

$$\begin{cases} \Lambda^{-1} = c'/c^2 \\ w = 2K/c \\ \xi = \sqrt{K \cdot A_{\text{crit}}}, \end{cases} \tag{4.2}$$

where the conduction velocity c, which depends on DI D, and its derivative $c' = dc/dD$ are both evaluated at the critical value D_{crit}. If an ionic model for the single cell is given, the parameters w, ξ, and Λ will depend on K only. Roughly speaking, c and c' are both proportional to $K^{1/2}$ (this may be understood easily by the example of two-current model, see Appendix of Ref. 19). Therefore, $w \sim K^{1/2}$, $\xi \sim K^{1/2}$, and $\Lambda^{-1} \sim K^{-1/2}$, and the dimensionless $\bar{\Lambda}^{-1} = \Lambda^{-1} \cdot \xi^4/w^3$ is almost not affected by K. Parameter σ defined in Eq. (2.4) does not depend on K, and $\bar{\sigma} = \sigma \cdot \xi^2/w^2$ will not be affected by K much either. However, the dimensionless cable length $\bar{\ell} = w\ell/\xi \sim K^{-1/2}$. Thus the dynamics of the modulation equation will be similar for various K, unless a significant change in $\bar{\ell}$ occurs. In one limit $K \to \infty$, we have $\ell \to 0$, which means the gap junctions between the cells are negligible and the fiber may be regarded as one single cell (if we ignore the intracellular resistance), and alternans are almost of constant amplitude along the cable; in the other limit $K \to 0$ we have a very large $\bar{\ell}$, and the extreme case $K=0$ indicates insulation between cells and propagation fails.

ACKNOWLEDGMENTS

We would like to thank Professor Henry Greenside for many useful discussions. We thank the referees for providing fruitful information and suggestions. This work is under the support of the National Institutes of Health under Grant No. 1R01-HL-72831 and the National Science Foundation under Grant No. PHY-0549259 and Agreement No. 0635561.

[1] J. N. Weiss, A. Garfinkel, H. S. Karagueuzian, Z. Qu, and P.-S. Chen, Circulation **99**, 2819 (1999).
[2] R. Pandit, A. Pande, S. Sinha, and A. Sen, Physica A **306**, 211 (2002).
[3] S. Alonso, F. Sagués, and A. S. Mikhailov, Science **299**, 1722 (2003).
[4] T. J. Lewis and M. R. Guevara, J. Theor. Biol. **146**, 407 (1990).
[5] H. M. Hastings, F. H. Fenton, S. J. Evans, O. Hotomaroglu, J. Geetha, K. Gittelson, J. Nilson, and A. Garfinkel, Phys. Rev. E **62**, 4043 (2000).
[6] Z. Qu, J. N. Weiss, and A. Garfinkel, Phys. Rev. Lett. **78**, 1387 (1997).
[7] A. Garfinkel, P. S. Chen, D. O. Walter, H. S. Karagueuzian, B. Kogan, S. J. Evans, M. Karpoukhin, C. Hwang, T. Uchida, M. Gotoh, O. Nwasokwa, P. Sager, and J. N. Weiss, J. Clin. Invest. **99**, 305 (1997).
[8] D. R. Chialvo, D. C. Michaels, and J. Jalife, Circ. Res. **66**, 525 (1990).
[9] A. Karma, Phys. Rev. Lett. **71**, 1103 (1993).
[10] A. Karma, Chaos **4**, 461 (1994).
[11] A. V. Panfilov, Chaos **8**, 57 (1998).
[12] R. F. Gilmour, Jr. and D. R. Chialvo, J. Cardiovasc. Electrophysiol. **10**, 1087 (1999).
[13] A. Garfinkel, Y.-H. Kim, O. Voroshilovsky, Z. Qu, J. R. Kil, M. Hyoung, H. S. Karagueuzian, J. N. Weiss, and P.-S. Chen, Proc. Natl. Acad. Sci. U.S.A. **97**, 6061 (2000).
[14] S. H. Hohnloser, T. Klingenheben, M. Zabel, Y.-G. Li, P. Albrecht, and R. J. Cohen, J. Cardiovasc. Electrophysiol. **8**, 987 (1997).
[15] D. Ruelle and F. Takens, Commun. Math. Phys. **20**, 167 (1971).
[16] D. Ruelle and F. Takens, Commun. Math. Phys. **23**, 343 (1971).
[17] S. Newhouse, D. Ruelle, and F. Takens, Commun. Math. Phys. **64**, 35 (1978).
[18] B. Echebarria and A. Karma, Phys. Rev. Lett. **88**, 208101 (2002).
[19] S. Dai and D. G. Schaeffer, SIAM J. Appl. Math. **69**, 704 (2008).
[20] J. B. Nolasco and R. W. Dahlen, J. Appl. Physiol. **25**, 191 (1968).
[21] B. Echebarria and A. Karma, Phys. Rev. E **76**, 051911 (2007).
[22] S. Dai and D. G. Schaeffer, "Bifurcations in a modulation equation for alternans in a cardiac fiber," Math. Modell. Numer. Anal. (to be published).
[23] M. R. Guevara, G. Ward, A. Shrier, and L. Glass, Proceedings of the 11th Computers in Cardiology Conference, IEEE Computer Society, Los Angeles, 1984, pp. 167–170.
[24] J. Guckenheimer and P. Holmes, *Nonlinear Oscillations, Dynamical Systems, and Bifurcations of Vector Fields* (Springer-Verlag, New York, 1983).
[25] N. Metropolis, M. L. Stein, and P. R. Stein, J. Comb. Theory, Ser. A, **15**, 25 (1973).
[26] K. T. Alligood, T. D. Sauer, and J. A. Yorke, *Chaos* (Springer-Verlag, New York, 2000).
[27] T. S. Parker and L. O. Chua, *Practical Numerical Algorithms for Chaotic Systems* (Springer-Verlag, New York, 2000).
[28] P. Grassberger and I. Procaccia, Phys. Rev. Lett. **50**, 346 (1983).
[29] S. H. Strogatz, *Nonlinear Dynamics and Chaos: With Applications to Physics, Biology, Chemistry, and Engineering* (Springer-Verlag, New York, 2000).
[30] P. Grassberger and I. Procaccia, Physica D **9**, 189 (1983).
[31] J. L. Kaplan and J. A. Yorke, Lect. Notes Math. **730**, 204 (1979).
[32] P. Frederickson, J. L. Kaplan, E. D. Yorke, and J. A. Yorke, J. Differ. Equations **49**, 185 (1983).
[33] F. Ledrappier and L. S. Young, Commun. Math. Phys. **117**, 529 (1988).
[34] L.-S. Young, Ergod. Theory Dyn. Syst. **2**, 109 (1982).
[35] D. Noble, J. Physiol. (London) **160**, 317 (1962).
[36] C. C. Mitchell and D. G. Schaeffer, Bull. Math. Biol. **65**, 767 (2003).
[37] L. Makowski, D. L. D. Caspar, W. C. Phillips, and D. A. Goodenough, J. Cell Biol. **74**, 629 (1977).
[38] J. P. Keener and J. Sneyd, *Mathematical Physiology* (Springer-Verlag, New York, 1998).